This is an open access article published under a Creative Commons Attribution (CC-BY) License, which permits unrestricted use, distribution and reproduction in any medium, provided the author and source are cited.

ACS AUTHORCHOICE

ACS OMEGA

http://pubs.acs.org/journal/acsodf

Article

Novel Strategy for Fabricating Multilayer Porous Membranes with Varying Porosity

Takafumi Aizawa*

Cite This: *ACS Omega* 2020, 5, 24461−24466

Read Online

ACCESS | Metrics & More | Article Recommendations

ABSTRACT: CO_2-assisted polymer compression (CAPC) is a method for fabricating porous polymer materials in which the polymer is plasticized with CO_2 and then pressed. In this work, a two-step molding method is adapted, and a porous membrane with multiple layers of varying porosity is fabricated by laminating sheets of a single starting material. A model is constructed in which the expansion owing to CO_2 and compression reflected by the longitudinal elastic modulus are considered. The model is constructed based on a two-layer experiment and extended to three layers. From the model simulation, the conditions for fabricating a multilayer porous polymer membrane with three layers of varying porosity (0.6, 0.5, and 0.4) and identical thickness (0.6 mm) are calculated. Finally, a porous membrane with varying porosity is fabricated based on the simulated design.

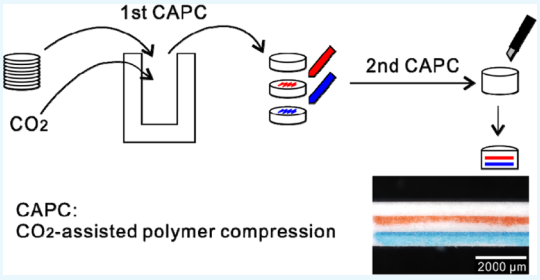

INTRODUCTION

Polymers are indispensable materials in daily life because of their lightweight and durable nature.[1] Among polymer materials, porous materials have numerous applications, such as filters, catalysts, bioreactors, and thermal insulators.[2] For example, porous fibrous materials are used for face masks,[3] 2.5 μm particulate matter filters,[4] water filters,[5] and filters for oil-in-water filtration.[6] In particular, nonwoven fabrics are often used in filters owing to their high productivity and low price.[7] These materials can also be functional; for example, porous membranes have been used as battery separators.[8] In the study of porous materials, obtaining a high-functionality material via precise manufacturing is the major theme.

The latest studies on the fabrication of porous polymer materials using CO_2 include injection molding with a mixture of CO_2,[9] fabrication by impregnating CO_2 into a solid polymer,[10] and polymeric membranes by supercritical CO_2-assisted phase inversion.[11]

In a previous study, a simple method for producing porous polymer materials was presented, in which fibrous sheets, such as nonwoven fabrics, were pressed by CO_2; this process was termed as CO_2-assisted polymer compression (CAPC).[12] The shape of the CAPC product is flexible and depends on the shape of the pressure vessel; moreover, the porosity and pore diameter can be controlled by the processing conditions.[13] The tunability of pore size of porous materials is crucial for practical use because pore geometry affects the diffusion in porous media.[14] The mechanical properties, such as the peel resistance and penetration resistance, of the CAPC products have been analyzed, and the peel resistance has been found to be well described by a cross-sectional analysis model that considers the aggregation of point adhesions in regions of overlapping fibers.[15] As an application for CAPC products, a tablet encapsulating a drug has been considered, and the drug release rate has been shown to be controllable.[16] Because CAPC is a batch process, productivity may be hindered. However, the productivity can be improved by utilizing an upscaling method in which multiple samples are simultaneously produced with a single press.[17]

As described above, CAPC has the significant advantage of controllability based on process conditions. However, when sheets of the same material are stacked and pressed together, a uniform porous membrane is produced. From the viewpoint of high-performance filter applications, pore diameters with gradient are desirable. Therefore, this study aimed to produce a porous membrane with multiple layers of varying porosity by laminating sheets of the same material. This study aims to establish a design method for multilayer filters comprising three layers with the same thickness and different porosities.

RESULTS AND DISCUSSION

A nonwoven fabric composed of poly(ethylene terephthalate) was used as a raw material sheet, and a three-layer porous membrane was established as a target, in which the layers obtained by stacking 10, 12, and 15 sheets have a constant

Received: June 17, 2020
Accepted: August 11, 2020
Published: September 14, 2020

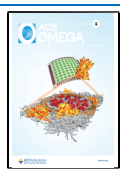

Downloaded via 65.21.193.86 on February 24, 2022 at 16:51:28 (UTC).
See https://pubs.acs.org/sharingguidelines for options on how to legitimately share published articles.

© 2020 American Chemical Society

https://dx.doi.org/10.1021/acsomega.0c02906
ACS Omega 2020, 5, 24461−24466

thickness. Because the target thickness of each layer is the same, a layer of 10 sheets should have a density that is two-thirds that of a 15-sheet layer with higher porosity. In addition, the relationship between the porosity and pore diameter has been previously reported;[13] thus, in a multilayer porous membrane, both the porosity and pore diameter are expected to decrease as the number of layers increases from 10 to 15 sheets.

If 37 sheets (total of 10, 12, and 15 sheets) are placed in a pressure vessel and subjected to CAPC, a uniform porous membrane should be formed, without a three-layer structure. Therefore, a two-step molding process is proposed in this work. The first CAPC product, which has a low density, is manufactured in the first step, and the final CAPC product, which has a three-layer structure, is fabricated by pressing the initially stacked CAPC products in the second step (Figure 1).

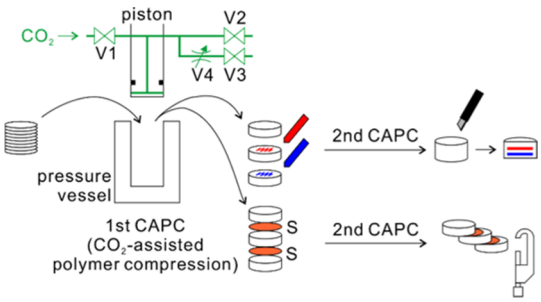

Figure 1. Fabrication of a multilayer porous material. V1: introduction valve, V2: exhaust valve, V3: exhaust valve, V4: metering valve, and S: separator. The procedure of preparing a cross-sectional sample for optical microscopy by coloring the intermediate and lower layers with felt-tip pens to (top), and the procedure of preparing a sample to determine the thickness of each layer with a micrometer caliper by suppressing adhesion and inserting separators between layers (bottom).

First, three CAPC products with a thickness of 0.7 mm were manufactured by compressing 10, 12, or 15 sheets. Based on the density (1.34 g mL^{-1}) provided in the datasheet, the thickness L_{solid} of a solid cylinder with 18 mm diameter is 0.238 mm at 0.081 g (10 sheets), 0.288 mm at 0.098 g (12 sheets), and 0.357 mm at 0.122 g (15 sheets). Regions with greater thicknesses were pores. Then, its porosity α can be derived from the calculated L_{solid} and its real thickness L_{porous} as follows

$$\alpha = \frac{L_{porous} - L_{solid}}{L_{porous}} \quad (1)$$

Hence, the porosity of first CAPC products with 0.7 mm thickness is 0.66, 0.59, and 0.49 for 10, 12, and 15 sheets, respectively.

Thereafter, the three samples were stacked, and the second CAPC process was performed to obtain a final CAPC product with a thickness of 1.8 mm. To clarify the layer boundaries, the surfaces of the middle and bottom samples were colored with a felt-tip pen before the second CAPC process. Figure 2 presents a microscopic image of the cross section of the fabricated product. The first layer, consisting of 10 sheets, corresponds to the top region of the red area, the second layer of 12 sheets is located in the top region of the blue area, and the third layer of 15 sheets accounts for the remaining regions. Obviously, the upper layer is compressed, indicating that a weaker layer with a lower density is more strongly compressed than the higher-density layer. Performing the second CAPC process at the same thickness

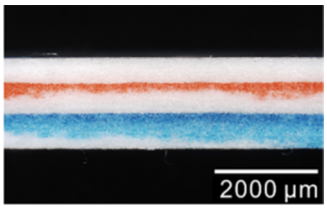

Figure 2. Optical microscopy image of the product cross section.

did not yield the desired results. For a strict analysis of the thickness, the adhesion between the layers was suppressed with polyimide films interposed between the layers, and the thickness of each layer was measured with a micrometer caliper. The layer thicknesses were found to be 0.50, 0.59, and 0.71 mm with the porosity of 0.52, 0.51, and 0.50, respectively. Because a layer with larger porosity compresses more strongly, the porosity of each layer becomes close due to this compression. As a trial, three CAPC products with thicknesses of 0.70 (10 sheets; porosity: 0.66), 0.65 (12 sheets; porosity: 0.56), and 0.60 mm (15 sheets; porosity: 0.41) were prepared, and the second CAPC process was used. The thicknesses of the final products were 0.54, 0.60, and 0.66 mm with the porosity of 0.56, 0.52, and 0.46, respectively. It was extremely difficult to produce a multilayer product with the same layer thickness by trial and error, suggesting the need for a design method. In both cases, the bottom layer (15 sheets) after the CAPC process is thicker than the initial sample, indicating that expansion occurred during the CAPC treatment.

Before considering a three-layer compression, a two-layer compression was analyzed. First, the CAPC treatment was performed by stacking 64 sheets to produce 2, 3, 4, and 5 mm samples. Figure 3 shows a scanning electron microscopy image

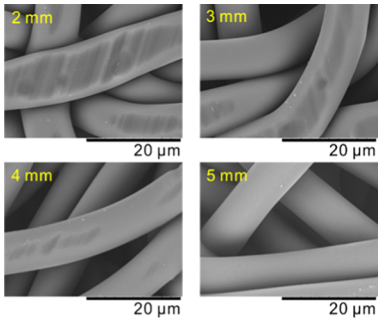

Figure 3. Scanning electron microscopy images of the surfaces of 64 nonwoven fabric sheets after the first CO_2-assisted polymer compression step. The sample thicknesses after compression are shown in the images.

of the sample surfaces. The fiber surface was compressed by being pushed by the bottom of the piston, and the compression region became larger as the compression progressed to 5, 4, 3, and 2 mm. Note the part on the left side of the 2 mm image where the fibers overlap each other in a cross shape. The origin of CAPC adhesion is point adhesion, in which the overlapping portions of fibers are deformed to cause crimping. In a previous study in which the adhesive strength was evaluated by changing the compressibility, it has been reported that adhesive strength can be explained by the analysis of aggregation of point adhesive.[15] Even in the case of the 2 mm sample, the fiber remains on the surface, and it is expected that the fiber-to-fiber

https://dx.doi.org/10.1021/acsomega.0c02906
ACS Omega 2020, 5, 24461−24466

overlapping portions will be combined by the second CAPC treatment.

It is necessary for the polymer to be sufficiently plasticized to deform so that the fibers would crimp together. Fibers do not bond in the absence of CO_2. CO_2 dissolves in the amorphous part of the polymer.[18] Differential scanning calorimetry measurement results of the raw fiber, first CAPC product, and second CAPC product are shown in Figure 4. The peak of

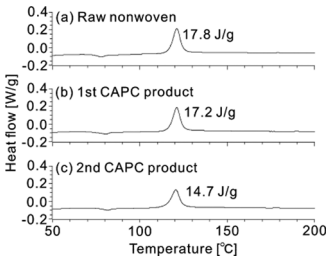

Figure 4. Differential scanning calorimetry data.

crystallization is observed at approximately 120 °C, which indicates that an amorphous portion exists. The peak slightly decreases each time the CAPC treatment is performed. This probably occurs because of CO_2-induced crystallization.[19]

A polyimide film was inserted between the CAPC samples with different thicknesses, and a second CAPC treatment was performed to assess the compression of each sample. The measurement was performed twice with the thinner sample at top and twice with the thinner sample at the bottom; the average values of the four experiments were used. The results are shown in Figure 5. In this figure, thick samples are indicated by positive

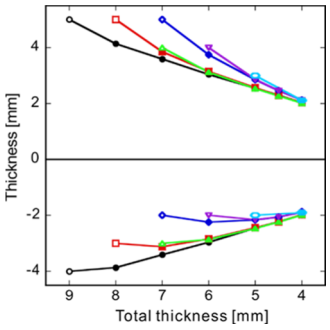

Figure 5. Compression results for two samples. The empty symbols indicate the initial sample thickness, and the filled symbols display the thickness of each layer with respect to the total thickness when the entire sample is subjected to CO_2-assisted polymer compression treatment. The standard deviation of each point fits within the symbol.

numbers and thin samples are indicated by negative numbers. The sum of the thicknesses of the two samples is the total thickness (x-axis). The empty symbols indicate the initial sample thickness, while the filled symbols show the sample thickness after the CAPC process. For example, note the black circle. The initial sample values are shown by hollow symbols (thicker sample: 5 mm, thinner sample: 4 mm) for a total of 9 mm along the x-axis. The stacked two samples were compressed to 8, 7, 6, 5.5, and 4 mm in the pressure vessel, and the thickness of each layer is indicated by the filled symbols. Similarly, the red squares show the results for the 5 and 3 mm samples compressed to 7, 6, 5.5, and 4 mm. Because the samples have the same weight, the thicker sample has a lower density. In Figure 5, the low-density sample results are given in the top panel, which demonstrates that the low-density samples are more compressed.

Next, the expansion of the samples was analyzed. Figure 6 shows the initial sample density and the expansion ratio for the

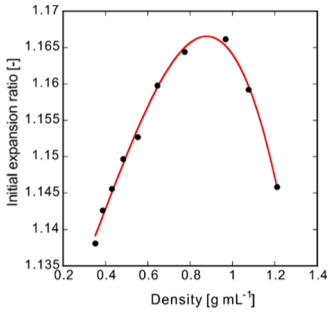

Figure 6. Measured expansion coefficient.

CAPC samples composed of 64 sheets with a thickness of 1.6–5.5 mm upon exposure to CO_2. It was found that the CAPC sample expanded upon exposure to CO_2.

Based on the above results, a model is proposed, as shown in Figure 7. When CO_2 is introduced during the initial stage of the

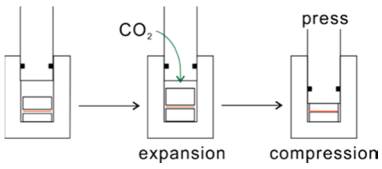

Figure 7. CO_2-assisted polymer compression model of compression after expansion.

CAPC procedure, the samples expand. Then, the expanded samples are compressed by the piston, and a compressed sample is formed. The initial expansion data in Figure 6 are measured after the sample is exposed to the atmosphere; thus, the data may be slightly different from the expansion data measured in the presence of CO_2. However, this difference may not be significant. The red line in Figure 6 presents fitting results obtained using the cubic equation with the least-squares method and the initial expansion. The initial expansion was assumed to follow a cubic equation. The sample compression should be related to the longitudinal elastic modulus of each layer, which must be a function of the density ρ of the porous material. According to Hooke's law, the stress σ is described as

$$\sigma = E(\rho)\varepsilon \tag{2}$$

based on the longitudinal elastic modulus $E(\rho)$ and strain ε.[20] The strain ε is obtained by dividing the compression length ΔL by the total length L. Let us consider how the total compression is distributed among each layer. When the cylinder is compressed from both ends, the stress of each layer in the cylinder is equal; thus, we have the following relationship

$$\sigma = E_1(\rho)\epsilon_1 = E_2(\rho)\epsilon_2 \tag{3}$$

Using the following definition and relationship

$$\epsilon_1 = \frac{\Delta L_1}{L_1} \tag{4}$$

https://dx.doi.org/10.1021/acsomega.0c02906
ACS Omega 2020, 5, 24461−24466

$$\epsilon_2 = \frac{\Delta L_2}{L_2} \tag{5}$$

$$\Delta L = \Delta L_1 + \Delta L_2 \tag{6}$$

the compression length of each layer was derived as follows

$$\Delta L_1 = \Delta L \frac{L_1}{E_1(\rho_1)} \frac{1}{\frac{L_1}{E_1(\rho_1)} + \frac{L_2}{E_2(\rho_2)}} \tag{7}$$

$$\Delta L_2 = \Delta L \frac{L_2}{E_2(\rho_2)} \frac{1}{\frac{L_1}{E_1(\rho_1)} + \frac{L_2}{E_2(\rho_2)}} \tag{8}$$

ΔL must be small because compression influences the sample density and $E(\rho)$. Therefore, in the simulation, the compression was performed in steps of 1 μm. For example, to achieve a compression of 2 mm, a compression of 1 μm was repeated 2000 times. To understand this further, consider a case where the thicknesses of the upper and lower samples are 3 and 2 mm, respectively. The initial expansion occurs according to the density of each sample, and if the upper and lower samples expand 1.15 and 1.16 times, the thicknesses of the upper and lower samples become 3.45 and 2.32 mm, respectively, after the introduction of CO_2. In the case of compression to a total of 4 mm, the total thickness of 5.77 mm will be reduced to 1.77 mm. According to eqs 7 and 8, the compression process is conducted in 1770 steps with 1 μm compression in each step.

The longitudinal elastic modulus $E(\rho)$ was determined by approximation to the fifth order, as follows. First, the initial samples are subjected to an initial expansion, which is described by a cubic equation. Then, the compression of each layer is calculated from the layer thickness and the longitudinal elastic modulus described by the quintic equation as a function of the layer density. Compression steps of 1 μm are repeated until the entire thickness reaches the target thickness. This step was performed by fitting the coefficient of the cubic initial expansion equation and the coefficient of the quintic longitudinal elastic modulus equation to match the experimental results in Figure 5. Fitting was conducted using the least-square method. Because it is difficult to determine derivatives under repetitive compression, the fitting was performed by the Downhill Simplex method,[21,22] which does not require derivatives. First, the initial expansion is fixed, as shown in Figure 6, and the fifth-order coefficient of the elastic modulus, which depends on the density, is determined by the fitting. Subsequently, the third-order coefficient of the initial expansion and the fifth-order coefficient of the longitudinal elastic modulus are determined, where the first fitting result is set as the initial value to perform the fitting.

Figure 8 presents plots of a cubic equation for the initial expansion and a quintic equation for the longitudinal elastic modulus, as determined by the fitting. Because only relative values are important for the longitudinal elastic modulus, a value was normalized by the value at a density of 1 g mL^{-1}. The initial expansion is not significantly different from that shown in Figure 6, and the fitting form appears to be accurate, with the longitudinal elastic modulus strongly increasing with increasing density.

The compression-after-expansion model was expanded from two-layer compression to three-layer compression. Using the expanded model, a compression of 0.7 (10 sheets), 0.7 (12 sheets), and 0.7 mm (15 sheets) was calculated as 0.51, 0.60, and 0.69 mm, respectively. The experimental data show good agreement with the model results. In addition, a compression of 0.7 (10 sheets), 0.65 (12 sheets), and 0.6 (15 sheets) was calculated as 0.55, 0.61, and 0.64 mm, respectively. These values are close to the experimental results, thus validating the model.

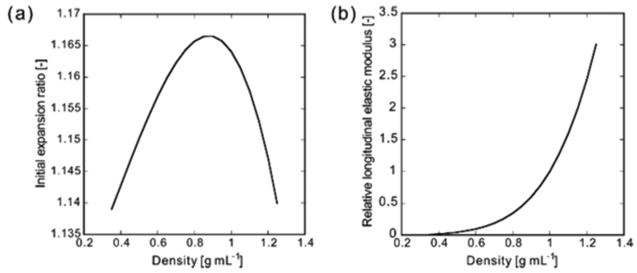

Figure 8. Fitting results. (a) Initial expansion determined by the fitting. (b) Longitudinal elastic modulus determined by the fitting.

After the simulation model was established, the initial sample thicknesses were varied to identify a combination in which each layer is 0.6 mm thick. Unlike the experimental results, the simulated results were obtained immediately, and although the input values were changed manually, with repeated calculations, the desired combination was found in a short period of time. When the CAPC treatment was simulated for samples with thicknesses of 0.738 (10 sheets; porosity: 0.68), 0.574 (12 sheets; porosity: 0.50), and 0.538 mm (15 sheets; porosity: 0.34), each layer was found to have a thickness of 0.60 mm. Based on this result, samples of 0.74, 0.57, and 0.54 mm were applied, which are close to the calculation results, and the samples of 0.61, 0.60, and 0.59 mm were produced with the porosity of 0.61, 0.52, and 0.39, respectively, thus validating the model. The results are summarized in Table 1. Figure 9 shows a cross section of the obtained sample. Each layer has equal thickness, indicating that the desired multilayer porous material was fabricated.

■ CONCLUSIONS

Using the CAPC treatment in two steps, multilayered porous structures with varying porosity were successfully fabricated. To design the desired multilayered porous membrane, a compression-after-expansion model was constructed in which compression was performed after an initial expansion by CO_2, while considering the longitudinal elastic modulus. The simulation and experimental results show good agreement. Although this study was conducted for three layers, this model can be easily extended to four or more layers and is extremely effective for designing multilayer filters using CAPC.

■ EXPERIMENTAL SECTION

The fiber sheets used in this study were composed of a poly(ethylene terephthalate) nonwoven fabric (fiber diameter: 8 μm, basis weight: 30 g m^{-2}) manufactured by Nippon Nozzle Co. Poly(ethylene terephthalate) pellets (model number: TK3) were supplied by Bell Polyester Products, Inc. The nonwoven fabric was punched into 18.0 mm circles. The sample weights were 0.081 g for 10 sheets, 0.098 g for 12 sheets, 0.122 g for 15 sheets, and 0.521 g for 64 sheets.

The CAPC process is illustrated in Figure 1, based on a press machine (JP-1504, Janome Sewing Machine, Co.). A piston with an outer diameter of 19.5 mm and an O-ring was attached on the side of the piston, and a sample was placed in a pressure vessel with an inner diameter of 20.0 mm. The experiments were performed at room temperature. The processing procedure is as follows. In the initial state, the valves are V1: closed, V2: open,

https://dx.doi.org/10.1021/acsomega.0c02906
ACS Omega 2020, 5, 24461−24466

Table 1. Summary of Experimental and Model Calculation Results of Three-Layer CO_2-Assisted Polymer Compression[a]

		before CAPC		after CAPC		model calculation	
sample no.	weight [g]	thickness [mm]	porosity [−]	thickness [mm]	porosity [−]	thickness [mm]	porosity [−]
1	0.081	0.70 ± 0.01	0.66	0.50 ± 0.01	0.52	0.51	0.53
	0.098	0.70 ± 0.01	0.59	0.59 ± 0.01	0.51	0.60	0.52
	0.122	0.70 ± 0.01	0.49	0.71 ± 0.01	0.50	0.69	0.48
2	0.081	0.70 ± 0.01	0.66	0.54 ± 0.01	0.56	0.55	0.57
	0.098	0.65 ± 0.01	0.56	0.60 ± 0.01	0.52	0.61	0.53
	0.122	0.60 ± 0.01	0.41	0.66 ± 0.01	0.46	0.64	0.47
3	0.081	0.74 ± 0.01	0.68	0.61 ± 0.01	0.61	0.60	0.60
	0.098	0.57 ± 0.01	0.50	0.60 ± 0.01	0.52	0.60	0.52
	0.122	0.54 ± 0.01	0.34	0.59 ± 0.01	0.39	0.60	0.41

[a]The error of thickness is standard deviation of six experiments.

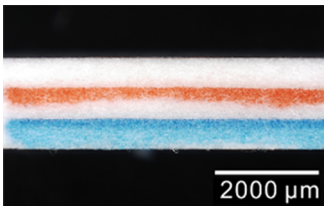

Figure 9. Optical microscopy image of the cross section of a multilayer porous material with the same thickness for each layer, as designed by the compression-after-expansion model.

and V3: closed. After a sample is placed in the pressure vessel, the piston is moved to a lower position to introduce CO_2. After V2 is closed, V1 is opened to introduce CO_2 through the piston shaft from the CO_2 cylinder. Then, V1 is closed and V2 is opened to release CO_2. Through this procedure, the air inside the pressure vessel is replaced with CO_2. Thereafter, V2 is closed, V1 is opened, and gaseous CO_2 is introduced at vapor pressure (6 MPa). After V1 is closed, the piston is lowered to the press position and pressed for 10 s. During the initial CAPC process, the sample is removed after V2 is opened, with a rapid release of CO_2 to the atmosphere. When multiple samples are combined in the CAPC process (second CAPC in Figure 1), V3 is opened with a slow release of CO_2 through the V4 metering valve (Swagelok Inc., SS-SS1) for 30 s; then, V2 is opened. The press position approximately matches the product thickness. When separators are inserted, the press position is adjusted to a higher position based on the total thickness of separators.

In this study, it is important to know the thickness of each layer. Therefore, when samples were prepared for optical microscopy, before the second CAPC treatment, the sample surfaces were colored with red and blue felt-tip pens, indicating the layer boundaries. To measure the thickness of each layer, a polyimide film with a thickness of 125 μm was interposed between the samples, and the sample was pressed under conditions in which the layers did not adhere to each other. Because polyimide is a polymer that cannot be plasticized by CO_2, the polyimide film can be used as a separator in the CAPC method (S in Figure 1). The thickness of each layer was measured by determining the center of the sample using a micrometer caliper. The average of six experiments is shown for the three-layer sample in the main text, and the average of four experiments is shown for the two-layer experiment.

To measure the initial expansion, after the CO_2 was introduced, the piston was moved 1 mm higher than the sample thickness; then, V2 was opened and immediately exhausted. This experiment was performed five times.

An RH-2000 (Hirox Co., Ltd.) optical microscope was used for cross-sectional imaging, and a TM-1000 scanning electron microscope (Hitachi High-Technologies) was used to observe the sample surfaces. Differential scanning calorimetry measurements were performed using Thermo Plus Evo DSC 8230 (Rigaku Co.) to explore the crystallinity.

■ AUTHOR INFORMATION

Corresponding Author

Takafumi Aizawa − *Research Institute for Chemical Process Technology, National Institute of Advanced Industrial Science and Technology, Sendai 983-8551, Japan;* orcid.org/0000-0003-3797-2279; Email: t.aizawa@aist.go.jp

Complete contact information is available at: https://pubs.acs.org/10.1021/acsomega.0c02906

Author Contributions

All experiments, model development, and analyses were conducted by T.A.

Notes

The author declares no competing financial interest.

■ REFERENCES

(1) Young, R. J.; Lovell, P. A. *Introduction to Polymers*, 3rd ed.; CRC Press, 2011.

(2) Ishizaki, K.; Komarneni, S.; Nanko, M. *Porous Materials: Process Technology And Applications*; Springer-Science+Business Media, 2014.

(3) Wang, N.; Cai, M.; Yang, X.; Yang, Y. Electret nanofibrous membrane with enhanced filtration performance and wearing comfortability for face mask. *J. Colloid Interface Sci.* **2018**, *530*, 695−703.

(4) Yang, X.; Pu, Y.; Li, S.; Liu, X.; Wang, Z.; Yuan, D.; Ning, X. Electrospun polymer composite membrane with superior thermal stability and excellent chemical resistance for high-Efficiency PM2.5 capture. *ACS Appl. Mater. Interfaces* **2019**, *11*, 43188−43199.

(5) Zhou, Z.; Lin, W.; Wu, X. F. Electrospinning ultrathin continuous cellulose acetate fibers for high-flux water filtration, Colloids and Surfaces A: Physicochem. *Colloids Surf., A* **2016**, *494*, 21−29.

(6) Agyemang, F. O.; Li, F.; Momade, F. W. Y.; Kim, H. Effect of poly(ethylene oxide) and water on electrospun poly(vinylidene fluoride) nanofibers with enhanced mechanical properties as pre-filter for oil-in-water filtration. *Mater. Chem. Phys.* **2016**, *182*, 208−218.

(7) Hutten, I. M. *Handbook of Nonwoven Filter Media*, 2nd ed.; Butterworth-Heinemann, 2016.

(8) Li, Y.; Li, Q.; Tan, Z. A review of electrospun nanofiber-based separators for rechargeable lithium-ion batteries. *J. Power Sources* **2019**, *443*, No. 227262.

(9) Wang, L.; Wakatsuki, Y.; Hikima, Y.; Ohshima, M.; Yusa, A.; Uezono, H.; Naitou, A. Preparation of microcellular injection-molded

foams using different types of low-pressure gases via a new foam injection molding technology. *Ind. Eng. Chem. Res.* **2019**, *58*, 17824−17832.

(10) Wang, J.; Chai, J.; Wang, G.; Zhao, J.; Zhang, D.; Li, B.; Zhao, H.; Zhao, G. Strong and thermally insulating polylactic acid/glass fiber composite foam fabricated by supercritical carbon dioxide foaming. *Int. J. Biol. Macromol.* **2019**, *138*, 144−155.

(11) Baldino, L.; Cardea, S.; Reverchon, E. Biodegradable membranes loaded with curcumin to be used as engineered independent devices in active packaging. *J. Taiwan Inst. Chem. Eng.* **2017**, *71*, 518−526.

(12) Aizawa, T. A new method for producing porous polymer materials using carbon dioxide and a piston. *J. Supercrit. Fluids* **2018**, *133*, 38−41.

(13) Aizawa, T. Fabrication of porosity-controlled polyethylene terephthalate porous materials using a CO_2-assisted polymer compression method. *RSC Adv.* **2018**, *8*, 3061−3068.

(14) Barman, S.; Rootén, H.; Bolin, D. Prediction of diffusive transport through polymer films from characteristics of the pore geometry. *AIChE J.* **2019**, *65*, 446−457.

(15) Aizawa, T. Peel and penetration resistance of porous polyethylene terephthalate material produced by CO_2-assisted polymer compression. *Molecules* **2019**, *24*, No. 1384.

(16) Wakui, Y.; Aizawa, T. Analysis of sustained release behavior of drug-containing tablet prepared by CO_2-assisted polymer compression. *Polymers* **2018**, *10*, No. 1405.

(17) Aizawa, T. Process development of CO_2-assisted polymer compression for high productivity: Improving equipment and the challenge of numbering-up. *Technologies* **2019**, *7*, No. 39.

(18) Kikic, I. Polymer−supercritical fluid interactions. *J. Supercrit. Fluids* **2009**, *47*, 458−465.

(19) Liao, X.; Nawaby, A. V. The sorption behaviors in PLLA-CO_2 system and its effect on foam morphology. *J. Polym. Res.* **2012**, *19*, No. 9827.

(20) Fried, J. R. *Polymer Science & Technology*, 3rd ed.; Prentice Hall, 2013.

(21) Press, W. H.; Teukolsky, S. A.; Vetterling, W. T.; Flannery, B. P. *Numerical Recipes*, 3rd ed.; The Art of Scientific Computing. Cambridge University Press, 2007.

(22) Nelder, J. A.; Mead, R. A simplex-method for function minimization. *Comput. J.* **1965**, *7*, 308−313.

https://dx.doi.org/10.1021/acsomega.0c02906
ACS Omega 2020, 5, 24461−24466